

# A Glycol/Water Co-Condensation Model to Investigate the Influence of Monoethylene Glycol on Top-of-the-Line Corrosion

Shaoqiang Guo,<sup>\*\*\*</sup> Fernando Farelas,<sup>\*</sup> and Marc Singer<sup>†,\*</sup>

## ABSTRACT

A mechanistic model was developed to predict the co-condensation of water and monoethylene glycol (MEG) at the top of a wet gas pipeline. The dropwise condensation process of water and MEG in the presence of noncondensing gas (CO<sub>2</sub>) is modeled based on a set of equations that describe the simultaneous heat and mass transfer to the condensed droplets. The model can predict the MEG concentration in the condensing phase, and the condensation rate of water and MEG. The accuracy of the model predictions was evaluated by comparison with flow loop experimental data. The results showed a decrease in condensation rate and increase of MEG content in the condensing phase with the increase of MEG content at the bottom of line. However, this effect is not significant unless the MEG content in the bottom liquid phase is higher than 70 wt%. Long-term corrosion experimental results showed that the presence of 50 wt% and 70 wt% MEG at the bottom liquid phase has a minimal effect on the top-of-the-line corrosion (TLC) rate, while the presence of 90 wt% MEG decreases the TLC rate significantly due to a sharp change of both condensation rate and the MEG content in the condensing phase.

**KEY WORDS:** carbon dioxide, condensation, mechanistic model, monoethylene glycol, top-of-the-line corrosion

## INTRODUCTION

For economic reasons and operational flexibility, unprocessed wet gas is often directly transported in subsea pipelines to onshore processing plants for dehydration, rather than being dried on offshore platforms. During the wet gas transportation, the water vapor in the hot gas stream will condense on the internal pipe wall due to the cooler outside environment. The dissolution of corrosive gases such as carbon dioxide (CO<sub>2</sub>) and hydrogen sulfide (H<sub>2</sub>S) in the condensed water can cause severe corrosion problems on the pipe wall. Top-of-the-line corrosion (TLC) can be a more serious concern than the bottom-of-the-line corrosion in oil and gas industry because: first, continuous condensation of water vapor constantly dilutes the dissolved iron ion in the condensed water droplets and challenges the formation of the protective corrosion product layer such as FeCO<sub>3</sub> in CO<sub>2</sub> corrosion environment; second, traditional corrosion inhibitors which are injected into the liquid phase at the bottom of line are often nonvolatile and cannot reach the condensed water at the top of the line.

So far, most research has been focused on various parameters influencing TLC such as condensation rate, temperature, flow velocity, CO<sub>2</sub> and H<sub>2</sub>S partial pressures, and acetic acid concentration, as well as amines.<sup>1-8</sup> However, results on the effect of monoethylene glycol (MEG) on TLC have been less publicized. In fact, large amounts of MEG are often injected in subsea wet gas pipelines as a hydrate inhibitor. The subsea wet gas pipelines with its typical operational pressure have a potential risk of gas hydrate formation

Submitted for publication: November 15, 2016. Revised and accepted: January 25, 2017. Preprint available online: January 26, 2017. <http://dx.doi.org/10.5006/2335>.

<sup>†</sup> Corresponding author. E-mail: singer@ohio.edu.

<sup>\*</sup> Institute for Corrosion and Multiphase Technology, Ohio University, 342 W. State St., Athens, OH 45701.

<sup>\*\*</sup> Corrosion and Protection Center, Institute for Advanced Materials and Technology, University of Science and Technology Beijing, Beijing 100083, PR China.

which can plug the pipeline and stop flow.<sup>9</sup> Typically, “lean MEG” (about 70 wt% to 90 wt% MEG) is injected offshore into the pipeline and transferred with water and natural gas. The MEG content in the bottom of the line will be first reduced by mixing with formation water. Further dilution will also occur all along the pipeline due to the condensation of the water vapor from the gas phase. A minimum MEG content of around 30 wt% to 50 wt% (“rich MEG”) at the onshore end of the pipeline is usually maintained by adjusting the injection rate of MEG at the pipe inlet.<sup>10-11</sup>

Although it is not its primary function, glycol is also used as a corrosion inhibitor in some wet gas pipelines, and a summary of field experiences has been given by Crolet and Samaran.<sup>12</sup> Experimental results found that the CO<sub>2</sub> corrosion rate of carbon steel fully immersed in the liquid phase decreases with the increase of glycol concentration.<sup>11</sup> An empirical glycol reduction factor developed by de Waard, et al.,<sup>13</sup> is often used to estimate the inhibition effect of glycol on CO<sub>2</sub> corrosion. The inhibition effect of MEG on CO<sub>2</sub> corrosion might be attributed to the influences of MEG concentration on the CO<sub>2</sub> solubility and diffusivity in the solution as well as the solubility limit of FeCO<sub>3</sub>.<sup>14-16</sup> Although the mechanism of MEG inhibition of CO<sub>2</sub> corrosion is still not well understood, it is acknowledged that the CO<sub>2</sub> corrosion rate decreases with the increase of MEG concentration. Therefore, prediction of the MEG concentration in the condensing phase at the top of the line is important for the understanding of its effects on TLC.

It is also necessary to predict the condensation rate in the presence of MEG because the saturated vapor pressure of water can be significantly lowered when the water phase contains considerable amounts of MEG. However, limited information exists on the modeling of MEG and water co-condensation in the literature. Available models<sup>13,17-18</sup> assume that the MEG/water mixture in the condensing film at the top of line is in equilibrium with the vapor phase without clarifying if the vapor phase is the vapor in the bulk gas phase or the vapor in the gas boundary layer adjacent to the condensed liquid. This information is essential because the resistance to mass transfer of vapors in the boundary layer is significant when noncondensable gases such as CO<sub>2</sub> are present.<sup>19</sup> This means that the composition of the vapor in the boundary layer adjacent to the condensed liquid can be very different from the composition of the vapor in the bulk gas phase, resulting in different predictions of MEG concentration in the condensed phase when using different vapor-liquid equilibrium assumptions. Actually, the equilibrium existence has been confirmed between the condensed liquid phase and the adjacent gas at the interface instead of the bulk gas phase for multicomponent condensation in the presence of noncondensing gas.<sup>20-21</sup>

In this work, a mechanistic condensation model for the co-condensation of MEG and water is presented

on the basis of a dropwise condensation model originally developed for water in noncondensable gas mixture.<sup>19</sup> The co-condensation model predicts the water and MEG condensation rates as well as the MEG concentration in the condensed liquid phase. The model was verified by comparison with experiments conducted in a large-scale, high-temperature and high-pressure flow loop. Finally, the effect of MEG content at the bottom of the line on the TLC rate and localized corrosion was investigated by long-term flow loop tests.

## MONOETHYLENE GLYCOL/WATER CONDENSATION MODEL

Whether the condensation in TLC condition is filmwise or dropwise is a long-lasting question for condensation modeling. In fact, the dropwise condensation occurs at low heat flux or subcooling temperature and shifts to filmwise condensation at higher subcooling temperature. Although different modes of transition from dropwise shifts to filmwise are found, the heat flux always gradually falls down with subcooling temperature in the transition region after climbing to the highest value at a critical subcooling temperature in the dropwise region.<sup>22</sup> Once the filmwise region is reached, the trend of increasing heat flux with increasing subcooling temperature is resumed. However, this drop of heat flux or condensation rate with subcooling temperature in the transition region has never been reported from available TLC experimental results, indicating the condensation is either dropwise or filmwise condensation in the typical conditions for TLC in wet gas pipelines. Nevertheless, the investigation of the morphology of corroded steel surface and the direct observation of condensed droplets in steel pipe using in situ video camera seem to show clearly that the condensation of water at the top of the pipeline occurs in a dropwise condensation mode rather than a filmwise condensation mode.<sup>20,23</sup>

In the presence of MEG, evidence of dropwise condensation was also confirmed in TLC experiments, and some examples are given in Figures 1 and 2. In order to visually observe the condensation on steel surface, a series of 48 h TLC tests was conducted in a transparent glass cell at various MEG concentrations and subcooling conditions. Steel samples were mounted on the lid of the glass cell and cooled by the external heat exchanger made of copper coils. The photos of the samples' surfaces after tests are given in Figure 1. The patterns on the sample surface indicate that the steel surface was occupied by a group of droplets with different diameters ranging from the order of micrometer (as indicated by the scanning electron microscopy [SEM] image in Figure 2[a]) to millimeter (Figure 1). Examination of the SEM images of the samples taken from the 21 d large-scale loop tests also showed similar patterns, as shown in Figure 2(b).

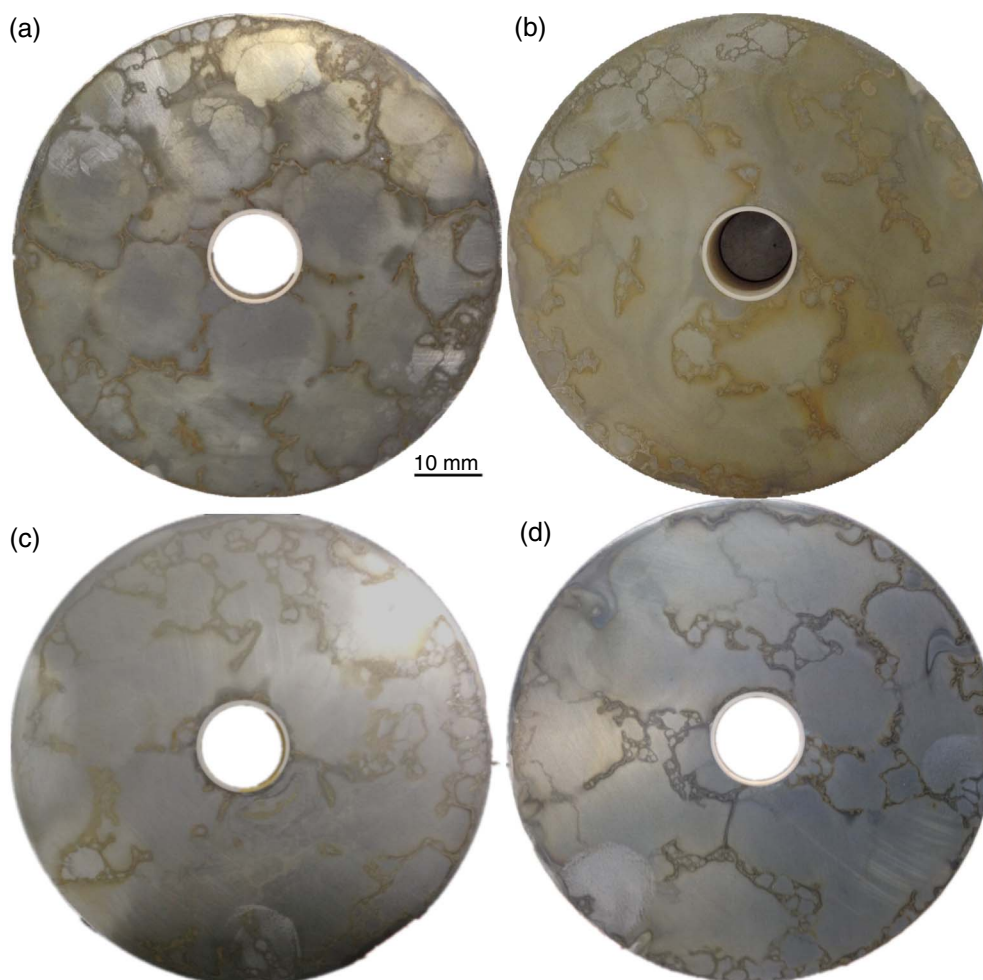


**FIGURE 1.** Evidence of dropwise condensation during MEG/water co-condensation: photos of samples after 48 h TLC tests in a glass cell setup. (a) 90 wt% MEG at low subcooling condition ( $T_{\text{gas}} = 65^{\circ}\text{C}$ ,  $T_{\text{sample}} = 40^{\circ}\text{C}$ ); (b), (c), and (d) 50 wt%, 70 wt%, and 90 wt% MEG at high subcooling condition ( $T_{\text{gas}} = 65^{\circ}\text{C}$ ,  $T_{\text{sample}} = 32^{\circ}\text{C}$ ), respectively.

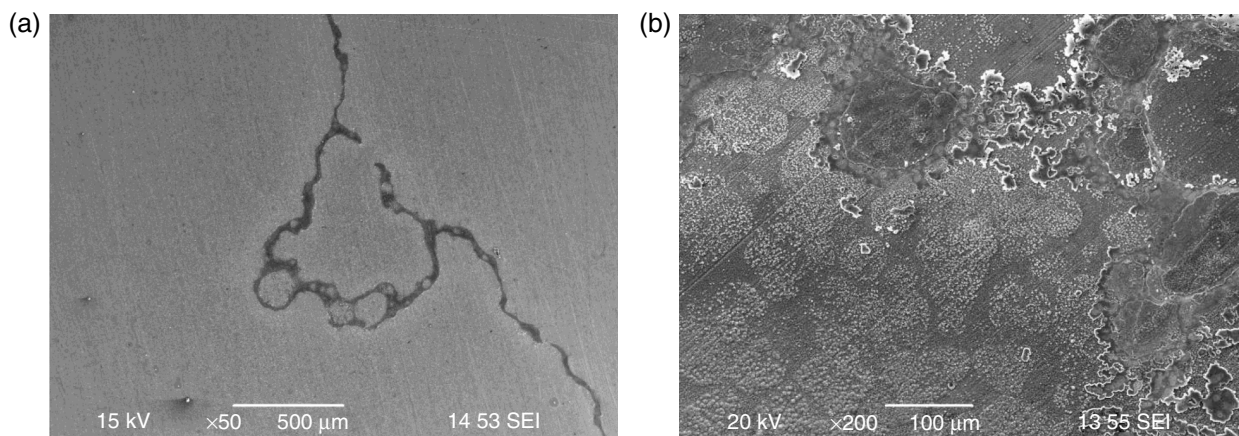


**FIGURE 2.** Evidence of dropwise condensation during MEG/water co-condensation: SEM images of sample surface after (a) 48 h glass cell test with 90 wt% MEG at  $T_{\text{gas}} = 65^{\circ}\text{C}$ ,  $T_{\text{sample}} = 32^{\circ}\text{C}$ ; and (b) 21 d loop test with 90 wt% MEG at  $T_{\text{gas}} = 42^{\circ}\text{C}$ ,  $T_{\text{sample}} = 40^{\circ}\text{C}$ .

This evidence indicates that the co-condensation of MEG and water is dropwise. In fact, the presence of MEG could lower the condensation rate and heat flux, so it is not surprising the co-condensation of MEG and water falls into the dropwise condensation region.

The co-condensation of MEG and water happens when the temperature of the outside environment is low enough to provide an inner pipe temperature below the saturation temperature of the vapor mixture. Zhang, et al.,<sup>19</sup> developed a comprehensive review on how to model the heat and mass transfer occurring in dropwise condensation in the presence of noncondensable gases. Only a summary of the modeling approach is described here, with an emphasis on the notable differences introduced due to the presence of MEG. In addition, as MEG is fully miscible with water at any ratio, each condensing droplet will contain a certain concentration of MEG when the water and MEG vapors condense at the top of the pipeline. A vapor-liquid equilibrium model must be incorporated to predict the phase composition.

### Heat Balance

A schematic representation of the dropwise co-condensation of MEG and water at the top of the wet gas pipeline and the temperature gradient in the gas boundary layer and a single droplet are shown in Figure 3. The heat is transferred from the bulk gas to the outside environment due to the temperature gradient. This gradient is also affected by the heat released due to the condensation of vapor to liquid.

The total heat exchange can be expressed as the sum of the heat loss through the gas boundary layer and the latent heat of phase change at the gas/droplet interface. The total heat flux ( $Q$ ) can be written as:

$$Q = Q_g + Q_c^1 + Q_c^2 \quad (1)$$

where  $Q_g$  is the heat flux through the gas boundary layer in  $W/m^2$ ;  $Q_c^1$  and  $Q_c^2$  are the latent heat flux by the condensation of water and MEG vapors at the droplet interface in  $W/m^2$ , respectively.

The heat flux  $Q_g$  through the gas boundary layer can be calculated from:

$$Q_g = h_g(T_b^g - T_i^g) \quad (2)$$

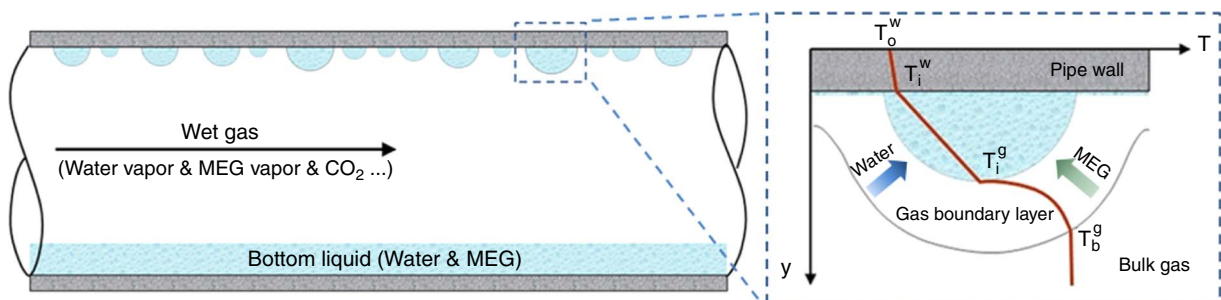


FIGURE 3. Dropwise condensation of water and MEG at top of the pipeline and temperature gradient in a single condensed droplet. (Adapted from Zhang, et al.<sup>19</sup>)

where  $h_g$  is the heat transfer coefficient for the gas boundary layer in  $W/m^2/K$  which can be estimated by the correlation  $Nu = 0.023 Re^{0.8} Pr^{0.4}$ ; Nusselt number  $Nu = h_g L / k_g$ ; Reynolds number  $Re = \rho_g v_g L / \mu_g$ ; Prantl number  $Pr = C_p \mu_g / k_g$ ;  $L$  is the characteristic length in  $m$ ;  $k_g$  is the thermal conductivity of the gas in  $W/m/K$ ;  $\rho_g$  is the gas density in  $kg/m^3$ ;  $v_g$  is the velocity of the gas in  $m/s$ ;  $\mu_g$  is the dynamic viscosity of gas in  $Pa \cdot s$ ;  $C_p$  is the heat capacity of gas in  $J/kg/K$ ;  $T_b^g$  is the temperature of the bulk gas in  $K$ ;  $T_i^g$  is the temperature of the gas at the droplet interface in  $K$ .

The latent heat fluxes  $Q_c^1$  and  $Q_c^2$  can be related to the water and MEG condensation rate, respectively:

$$Q_c^1 = R_c^1 H_c^1 \quad (3)$$

$$Q_c^2 = R_c^2 H_c^2 \quad (4)$$

where  $R_c^1$  and  $R_c^2$  are water and MEG condensation rate in  $kg/m^2/s$ , respectively;  $H_c^1$  and  $H_c^2$  are the latent heat of condensation for water and MEG in  $J/kg$ , respectively.

The total heat flux ( $Q$ ) considering a large number of droplets per unit area can be calculated through a statistical approach considering the droplet-size distribution:

$$Q = \int_{r_{\min}}^{r_{\max}} q(r) N(r) dr \quad (5)$$

where:  $r_{\min}$  and  $r_{\max}$  represent the minimum and maximum radius of droplets in  $m$ , respectively;  $q(r)$  represents the heat that passes through a single droplet of radius  $r$ , in  $W$ .

The number of droplets with a radius  $r$  per unit area can be calculated from the droplet size distribution  $N(r)dr$ :<sup>24</sup>

$$N(r)dr = \frac{1}{3\pi r_{\max}^2} \left( \frac{r}{r_{\max}} \right)^{-2/3} dr \quad (6)$$

The derivation of the heat  $q(r)$  transferred through a droplet of radius  $r$  is identical to the approach proposed by Zhang, et al.<sup>19</sup> Simplifying the situation to a one dimension heat transfer problem considering

multiple heat resistance (droplet, wall, insulation layer if any), the heat  $q(r)$  can be expressed:

$$q(r) = \frac{T_i^g \left( 1 - \frac{2\sigma}{H_i^m r} \right) - T^o}{\frac{1}{4\pi r k_d} + \frac{1}{2\pi r^2 h_i} + \frac{d_w}{4\pi r^2 k_w} + \frac{d_i}{4\pi r^2 k_i}} \quad (7)$$

where  $k_d$ ,  $k_w$ , and  $k_i$  represent the thermal conductivities of the droplet which is a mixture of MEG and water, of the pipe wall, and of the insulation layer, respectively, in W/m/K;  $\sigma$  is the surface tension of water and MEG mixture, in N/m;  $H_i^m$  is the latent heat released from the condensation of MEG and water mixture, in J/kg;  $\rho$  is the density of mixture of water and MEG at the droplet interface, in kg/m<sup>3</sup>;  $T^o$  is the temperature of the outer pipe wall, in K;  $d_w$  and  $d_i$  are the thickness of the pipe wall and the insulation layer respectively, in m.

Finally, combination of Equations (1) through (5) yields the final heat balance equation:

$$h_g(T_b^g - T_i^g) + R_c^1 H_c^1 + R_c^2 H_c^2 = \int_{r_{\min}}^{r_{\max}} q(r) N(r) dr \quad (8)$$

As displayed in Equation (8), there are three unknown variables: the temperature of the droplet interface  $T_i^g$ , the water condensation rate  $R_c^1$ , and MEG condensation rate  $R_c^2$ . The minimum and maximum radius of the condensed droplet can be determined by the methods described by Zhang, et al.<sup>19</sup> The variables related to the properties of the gas mixture and condensed liquid can be calculated at the appropriate temperature and pressure conditions using well-accepted correlations while the gas and condensed liquid compositions have to be estimated using, for example, the vapor-liquid equilibrium calculations introduced in a later section.

### Mass Balance

As all of the water condensing at the top of the line comes from the transportation of water vapor from the bulk gas phase to the gas/droplet interface, water condensation rate can be expressed as the mass transfer rate of water vapor through the boundary layer as:

$$R_c^1 = \rho_g \beta_g^1 (w_b^1 - w_i^1) \quad (9)$$

where  $\rho_g$  is the gas density in kg/m<sup>3</sup>;  $\beta_g^1$  is the mass transfer coefficient of water vapor in the gas in m/s;  $w_b^1$  and  $w_i^1$  are the mass fraction of water vapor in the bulk gas and at the gas/liquid interface, respectively.

Similarly, the MEG condensation rate  $R_c^2$  can be expressed as:

$$R_c^2 = \rho_g \beta_g^2 (w_b^2 - w_i^2) \quad (10)$$

where  $\rho_g$  is the gas density, in kg/m<sup>3</sup>;  $\beta_g^2$  is the mass transfer coefficient of MEG vapor in the gas, in m/s;  $w_b^2$

and  $w_i^2$  are the mass fraction of MEG vapor in the bulk gas and at the gas/liquid interface, respectively.

The mass transfer coefficient of water vapor or MEG vapor can be estimated by the correlation between heat transfer coefficient  $h_g$  and mass transfer coefficient  $\beta_g$ .<sup>25</sup>

$$\rho_g \beta_g = \frac{h_g}{C_p} Le^{-2/3} \quad (11)$$

where  $C_p$  is the heat capacity of the gas, in J/K/kg;  $Le = k_g / (\rho_g C_p D_v)$  is the Lewis number;  $D_v$  is the diffusivity of corresponding water vapor or MEG vapor in the gas boundary layer, in m<sup>2</sup>/s.

To solve the set of coupled heat and mass balance Equations (8) through (10), the vapor composition has to be known to obtain mass fractions of water and MEG vapors in Equations (9) and (10). The condensed liquid composition also needs to be known to calculate the condensed liquid properties such as  $k_d$ ,  $H_c^m$ , and  $\sigma$  in Equation (7).

### Vapor-Liquid Equilibrium

The calculations of the vapor composition in the bulk gas and at the gas/droplet interface are based on the following assumptions:

- The water/MEG liquid accumulated at the bottom of the pipeline is in equilibrium with the bulk gas phase at a same temperature  $T_b^g$ .
- At the top of the line, the vapor-liquid equilibrium exists at the gas/droplet interface, i.e., the water/MEG mixture condensing at the interface is in equilibrium with its adjacent gas at the interface temperature  $T_i^g$ .

The fraction of water vapor and MEG vapor in the bulk gas phase can be calculated by performing a flash calculation for vapor-liquid equilibrium at the bottom of the line. For the flash calculation, temperature of the bulk gas, total pressure and composition of the total fluid (including the bulk gas fluid and the liquid fluid at the bottom of line) are required. The composition of the total fluid can be estimated by the MEG concentration in the liquid phase at the bottom of line, liquid hold up, and also the produced natural gas composition which are usually known at a gas field. In the flash calculation, the Peng-Robinson (PR) equation of state (EoS) with the classical van der Waals mixing rules is used to calculate the water and MEG fugacity in the gas and liquid phase.

The PR equation of state contains two parameters:<sup>26</sup>

$$P = \frac{RT}{v-b} - \frac{a(T)}{v(v+b) + b(v-b)} \quad (12)$$

where  $P$ ,  $T$ , and  $V$  are pressure, temperature, and molar volume, respectively; the parameters  $a$  and  $b$  are expressed for the pure components as  $a = 0.45724(R^2 T_c^2 / P_c) \alpha$  and  $b = 0.0778(R T_c / P_c)$ ;

$\alpha^{1/2} = 1 + m(1 - T_r^{1/2})$ ;  $m = 0.37464 + 1.54226\omega - 0.26992\omega^2$ ;  $T_c$  is critical temperature for a pure component in K;  $P_c$  is critical pressure for a pure component in bar;  $\omega$  is the acentric factor;  $R = 0.08314 \text{ L}\cdot\text{bar}/\text{mol}\cdot\text{K}$ .

The fugacity of component  $j$ ,  $f_j$ , in a mixture can be calculated from the following equation:

$$\ln \frac{f_j}{x_j P} = \frac{b_j}{b} (Z - 1) - \ln(Z - B) - \frac{A}{2\sqrt{2}B} \left( \frac{2 \sum_i x_i a_{ij}}{a} - \frac{b_j}{b} \right) \ln \left( \frac{Z + 2.414B}{Z - 0.414B} \right) \quad (13)$$

where  $A = aP/R^2T^2$ ;  $B = bP/RT$ ;  $Z = Pv/RT$ .

For the mixture, the van der Waals mixing rules are used:

$$a = \sum_i \sum_j x_i x_j (1 - k_{ij}) (a_i a_j)^{1/2} \quad (14)$$

$$b = \sum_i x_i b_i \quad (15)$$

where  $a_i$  and  $b_i$  are parameters  $a$  and  $b$  in Equation (12) for component  $i$ ;  $x_i$  is the mole fraction of component  $i$  in liquid or vapor phase;  $k_{ij}$  is an empirical binary parameter for components  $i$  and  $j$ .

The critical temperature, critical pressure, and the acentric factor of water, MEG<sup>27</sup>, and CO<sub>2</sub> used in this work are listed in Table 1. Access to binary parameters for water/MEG/CO<sub>2</sub> system is limited and very different values are found in existing literature. Therefore, to simplify, the binary interaction parameters are set to zero. It should be mentioned that the MEG/water co-condensation model is not only limited to water/MEG/CO<sub>2</sub> system but can also be implemented to the case in which the other noncondensable gases are present. The hydrocarbons can also be incorporated in the model as other gas components if the hydrocarbons' vapor pressures are below saturation. The critical parameters and binary interaction parameters for hydrocarbon components in the natural gas can be found in literature.<sup>28</sup> In the case of hydrocarbons whose vapor pressures reach saturation, the condensation of hydrocarbons that are insoluble with water and MEG has to be considered. A co-condensation model for water and hydrocarbon has also been developed in the authors' group,<sup>29</sup> and can be combined with the MEG/water co-condensation model in this work for the multi-condensation process in a real wet gas pipeline using glycol as gas hydrate and/or corrosion inhibitor.

TABLE 1

Critical Temperatures ( $T_c$ ), Critical Pressures ( $P_c$ ), and Acentric Factors Used in the Model

| Components      | $T_c$ (K) | $P_c$ (bar) | Acentric Factor |
|-----------------|-----------|-------------|-----------------|
| Water           | 647.1     | 219.4       | 0.343           |
| MEG             | 720.0     | 82.0        | 0.507           |
| CO <sub>2</sub> | 304.2     | 73.9        | 0.224           |

Two criteria have to be followed for the flash calculation: one is the mass conservation for each component and the other is that the fugacity of each component in liquid and vapor phase has to be equal. The algorithm for flash calculation using the equation of state can be found from published literature.<sup>30-31</sup> By performing the flash calculation for vapor-liquid equilibrium at the bottom of line, the composition of bulk gas can be obtained. Then the mass fraction of water and MEG vapor in bulk gas phase, and also the gas properties such as density and heat capacity in the heat and mass transfer equations can be calculated.

Similarly, the flash calculation can also be conducted for the vapor-liquid equilibrium at the gas/droplet interface at top of the line. Here, the bulk gas phase is the feeding fluid, so the total fluid composition is set to be the bulk gas composition. If the interface temperature  $T_i^g$  is known, the composition of the gas and condensing liquid at the gas/droplet interface can be estimated by the second flash calculation, which means that the mass fraction of vapor at the interface in Equations (9) and (10) can be obtained.

Finally, three unknown variables remain i.e.,  $T_i^g$ ,  $R_c^1$ , and  $R_c^2$ , for three equations: (8), (9), and (10). A simplified algorithm for the solution is shown in Figure 4. The water and MEG condensation rate can be obtained, and the MEG concentration of the condensing liquid at top of the line is the ratio of MEG condensation rate to the total condensation rate of water and MEG.

## VALIDATION OF CONDENSATION MODEL

A large number of MEG/water co-condensation tests were conducted in a large-scale flow loop to verify

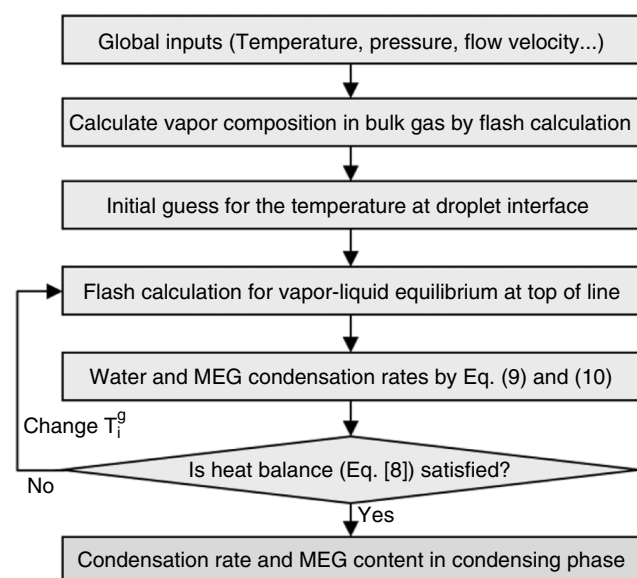


FIGURE 4. Flow chart for the numerical calculation in the co-condensation model.

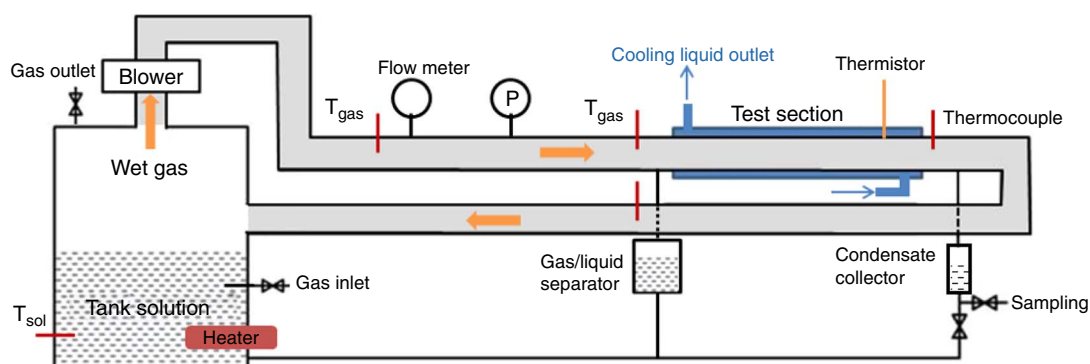


FIGURE 5. The schematic diagram of the large-scale TLC wet gas flow loop.

the proposed model predictions. The schematic diagram of the TLC flow loop is shown in Figure 5. The tank was filled with deionized (DI) water and MEG, and a heater immersed in the solution was used to generate the mixture of water and MEG vapors. CO<sub>2</sub> was added to the gas phase and a blower was used for the circulation of the wet gas. The 4 in. (10.16 cm) diameter flow loop was 30 m long and horizontally leveled. The test section was equipped with a cooling system so the temperature of the pipe wall could be controlled by changing the flow rate of the coolant. Thermocouples were used to monitor the gas temperature, while thermistors inside the pipe wall were used to monitor the pipe wall temperature. When the hot wet gas contacted the cold pipe wall in the test section, MEG/water co-condensation occurred and the condensed liquid in the test section was drained to a liquid collector located downstream. A transparent quartz column with scale marks was connected to the collector in order to monitor the level of the collected liquid column with time. The accumulation of condensed liquid in the column was converted to a total condensation rate. The collected condensed liquid was also sampled for analysis of the MEG concentration by gas chromatography. The ranges of the test parameters for the MEG/water co-condensation loop tests are listed in Table 2.

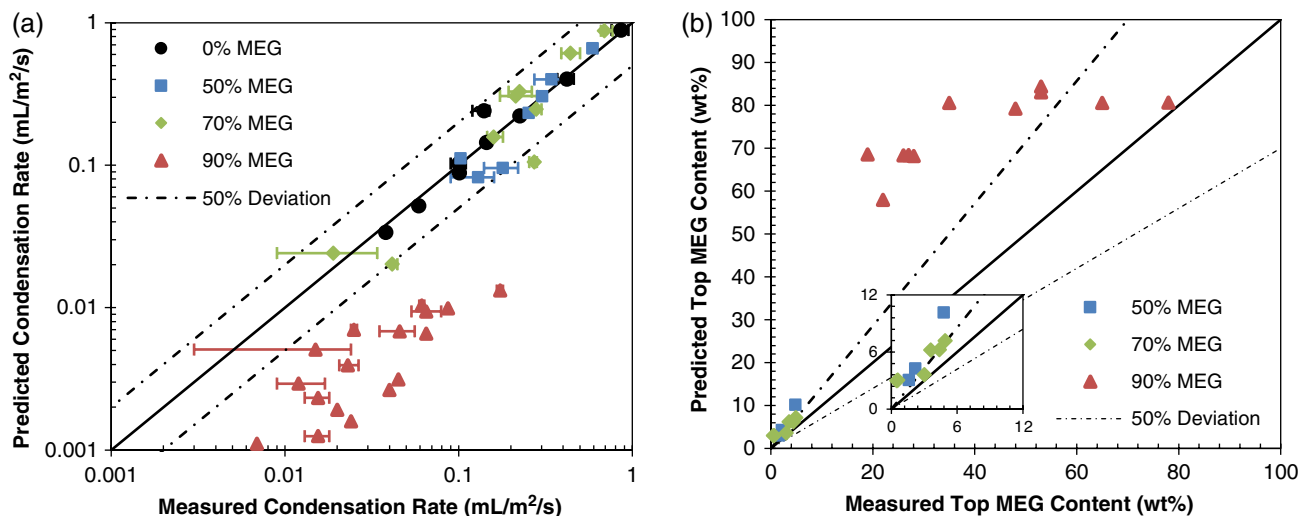
Figure 6(a) shows the comparison between the measured total condensation rate (including water and MEG) and the predicted total condensation rate. As shown in Figure 6(a), 30 of the 44 tests were replicated,

TABLE 2

Test Conditions of the MEG/Water Co-Condensation Test in the Large-Scale Flow Loop

| Variables                              | Range   |         |
|--|---------|---------|
|  | Minimum | Maximum |
| MEG content in tank solution (wt%)     | 0       | 90      |
| Total pressure, $P_{total}$ (bar)      | 1       | 3       |
| Gas temperature, $T_{gas}$ (°C)        | 42      | 67      |
| Pipe wall temperature, $T_{pipe}$ (°C) | 32      | 65      |
| Gas velocity, $v_{gas}$ (m/s)          | 1       | 3       |

and the error bars represent the maximum and minimum values of the measured condensation rate from the replicates. Seven data points (1 at 50 wt% MEG, 3 at 70 wt% MEG, and 3 at 90 wt% MEG) have very small error bars which can still be distinguished from the data marker. The 14 data points without error bars indicate that no replicate test was conducted. The condensation rate is plotted in logarithmic scale as the condensation rate with 90 wt% MEG at bottom of line is about 10 to 100 times lower than with other MEG concentrations. The MEG/water co-condensation model gives a good prediction of the condensation rate at MEG-free condition, indicating the compatibility of the proposed model with a water-only condensation situation. In the presence of 50 wt% and 70 wt% MEG at the bottom of line solution, the model predictions agree reasonably well with the experimental data. However, the calculated condensation rates are significantly lower than the test results for the 90 wt% MEG experiments, which corresponds to the overpredicted MEG concentration in condensing droplets at the top of the line as shown in Figure 6(b). This deviation is very likely caused by errors in the estimation of the vapor composition in the bulk gas phase, and can be linked to the vapor-liquid equilibrium calculations. During the flow loop tests, even though the tank and the whole loop were insulated with fiberglass material, a temperature drop from the liquid phase in the tank to the gas phase was observed and became notable when MEG content increased to 90 wt%. For comparison, the situation was simulated in a 2 L glass cell and the temperature gradients of the DI water and 90 wt% MEG solution are shown in Figure 7. The liquid temperature was controlled by the hot plate and one thermocouple, while the temperature at different depths was measured by another thermocouple. It can be seen that the temperature drop at the liquid/vapor interface becomes obviously larger in the presence of 90 wt% MEG in the bottom liquid phase. Therefore, it can be expected that a larger deviation of model prediction will be observed at higher MEG concentration like 90 wt%, as the evaluation of the vapor fraction in the bulk gas phase in



**FIGURE 6.** Comparison of the measured and predicted (a) condensation rate and (b) MEG content in condensing liquid at top of line.

the model is based on the assumption of the vapor-liquid equilibrium at the bottom of line. Nevertheless, the model shows good predictions when the MEG content is up to 70 wt% and succeeds on describing the co-condensation process of water and MEG in the

presence of noncondensable gases. In addition, the model predictions could be improved at 90 wt% MEG content if the vapor composition in the bulk gas phase can be directly measured or estimated in other ways instead of the equilibrium estimation.

In addition to the uncertainty caused by the equilibrium estimation, the prediction of the co-condensation model may lack accuracy at very high gas velocities where condensation mode may switch from dropwise to filmwise. Droplets may slide along the pipeline at higher velocity which may disorder the distribution of the droplets and leave a temporary continuous film along its sliding path. By considering the balance of gravity of the droplet, drag force by gas flow, surface tension, and other forces, the model can predict the critical flow velocity above which the falling droplet shifts to sliding droplets. This critical flow velocity can vary from 3 m/s to 7 m/s at different conditions.<sup>24</sup> Although this uncertainty is likely to be minor, the further validation of co-condensation model is necessary for its application at high velocities, i.e., sliding droplet region. The condensation tests conducted in this work are in the falling droplet region.

## EFFECT OF MONOETHYLENE GLYCOL CONTENT ON TOP-OF-THE-LINE CORROSION

### Experimental Method

Long-term TLC tests with various contents of MEG in the tank solution were performed in the large-scale flow loop shown in Figure 5. Three probes with weight loss samples, which were made of API 5L X65 pipeline material (composition in wt%, C 0.13, Mn 1.16, P 0.009, S 0.023, and Fe balance), were flush mounted to the top of the test section to study the effect of MEG on the corrosion behavior at the top of the line. Prior to the experiment, the whole system was

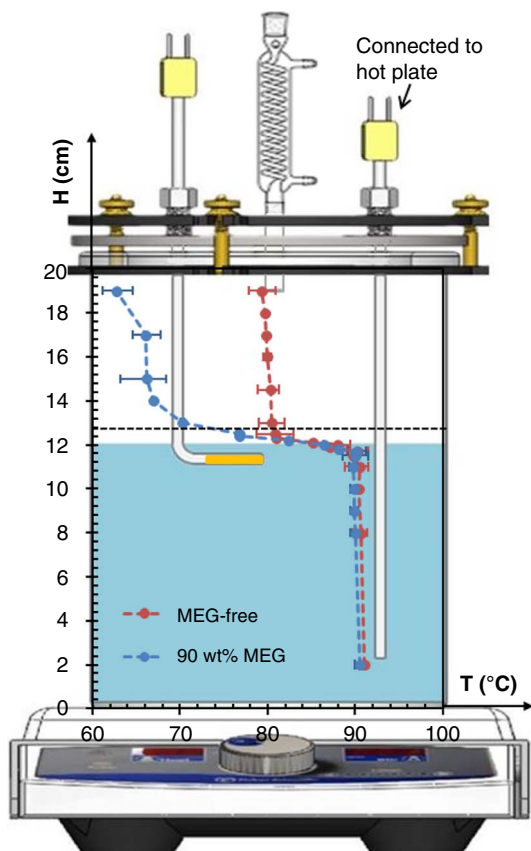


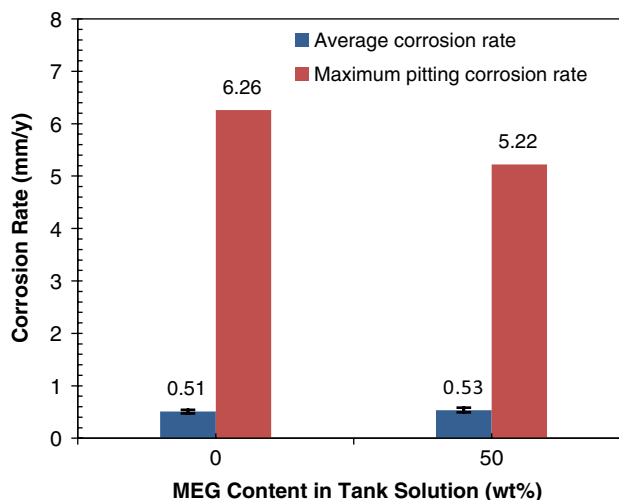
**FIGURE 7.** Temperature gradient from bottom liquid phase to gas phase for MEG-free solution and 90 wt% MEG solution.

deoxygenated by bubbling CO<sub>2</sub> gas in the tank solution until the O<sub>2</sub> concentration was lower than 40 ppb. The temperature of the pipe wall was controlled by adjusting the flow rate of the coolant in the copper coil surrounding the test section. After reaching steady state, i.e., desired temperature, flow velocity, pressure, and stable condensation rate, the weight loss probes were installed into the probe ports at the top of test section, and then the test was started.

The weight loss sample surface (except for the exposed surface) was coated with a thin layer of electrically insulating polymer coating. The exposed surface of corrosion samples with a diameter of 3.17 cm was subsequently ground with 360, 800, and 1200 grit silicon carbide paper, rinsed with DI water and isopropanol, and dried before they were mounted to the ports in the test section with specially designed sample holders. After completion of each test, the weight loss sample surface was prepared for SEM cross-section analysis. The corrosion products formed on the sample surface were then removed by exposure to inhibited acid solution (1,000 mL hydrochloric acid + 20 g antimony trioxide + 50 g stannous chloride), suggested by the ASTM G1-03 standard to calculate the average corrosion rate by weight loss. Localized corrosion morphology and corresponding pit distribution and pit depth were obtained by performing a surface analysis on each sample with a 3D surface profilometer.

### Influence of “Rich MEG” on Top-of-the-Line Corrosion

As “rich MEG” (30 wt% to 50 wt% MEG) is the minimum MEG content used to prevent the formation of gas hydrate, long-term (21 d) TLC test with 50 wt% MEG at bottom and without MEG were performed in the flow loop to investigate the “rich MEG” effect on TLC. Previous research<sup>32</sup> found that the presence of 50 wt% MEG had no effect on TLC as long as the condensation rate was kept constant by controlling the cooling condition. In this work, rather than trying to match the condensation rates between experiments, it was decided to control the pipe wall temperature instead. This approach was more effective in capturing the effect of MEG content on the entire process as the condensation and corrosion were in this case closely related. The gas temperature was 62°C, and the pipe wall temperature was controlled at 54°C. The gas velocity was 3 m/s. The total pressure was 3 bars, and the CO<sub>2</sub> partial pressure in bulk gas phase was 2.81 bars. The average corrosion rate and the maximum pitting corrosion rate after 21 d of corrosion are given in Figure 8. Although some decrease of the maximum pitting corrosion rate in the presence of 50 wt% MEG is seen in Figure 8, there was no evidence of a dramatic change in TLC rate and localized corrosion rate. This can be attributed to the little effect of “rich MEG” on condensation. As shown in



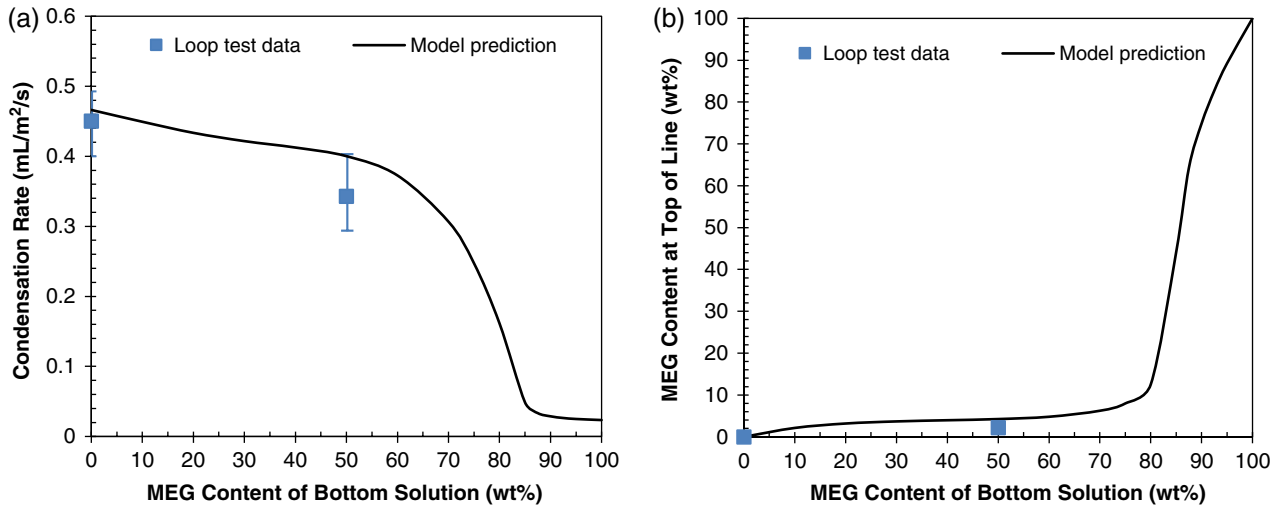
**FIGURE 8.** Effect of 50 wt% MEG on average TLC rate and maximum pitting corrosion rate ( $T_{\text{gas}} = 62^{\circ}\text{C}$ ,  $T_{\text{pipe}} = 54^{\circ}\text{C}$ ,  $P_{\text{total}} = 3 \text{ bar}$ ,  $v_{\text{gas}} = 3 \text{ m/s}$ , 21 d).

Figure 9, the experimental results showed that the presence of 50 wt% MEG only decreased the condensation rate about 18% in comparison with the condensation rate at MEG-free condition, and the MEG content in the condensed liquid was measured to be less than 3 wt%. The error bars in Figures 8 and 9(a) represent the maximum and minimum values of the measured corrosion/condensation rate from replicates.

The maximum pitting corrosion rate displayed in Figure 8 was calculated based on the maximum pitting depth observed in Figure 10. Figure 10 shows the pitting depth distribution of the sample from the 21 d loop test with 50 wt% bottom MEG content. Figure 10(a) depicts the sample surface after removal of the corrosion product layer, which presented signs of localized corrosion. The pitting depth distribution of the sample surface was analyzed using a profilometer as shown in Figures 10(b) and (c). It can be seen that the maximum pitting depth was about 340  $\mu\text{m}$ , corresponding to a pitting corrosion rate of 5.2 mm/y. The pitting ratio was also calculated by dividing the maximum pitting corrosion rate to the general corrosion rate. Generally, a high pitting ratio indicates severe pitting corrosion. The pitting ratio was 9.8 with 50 wt% MEG, indicating a clear occurrence of localized corrosion in the presence of 50 wt% MEG at the bottom of line. A similar pitting ratio of 12.3 in the MEG-free condition was obtained, and the detailed pitting depth profile was reported previously.<sup>33</sup>

### Influence of “Lean MEG” on Top-of-the-Line Corrosion

TLC is more severe at the beginning part of the wet gas pipeline due to the high condensation rate in the surrounded cold deep seawater conditions. In some wet gas pipelines, “lean MEG” is injected at the well head and a MEG concentration of 70 wt% to 90 wt% in the



**FIGURE 9.** Effect of 50 wt% MEG on (a) condensation rate and the (b) MEG concentration in the condensing liquid at top of line ( $T_{\text{gas}} = 62^{\circ}\text{C}$ ,  $T_{\text{pipe}} = 54^{\circ}\text{C}$ ,  $P_{\text{total}} = 3$  bar,  $v_{\text{gas}} = 3$  m/s, 21 d).

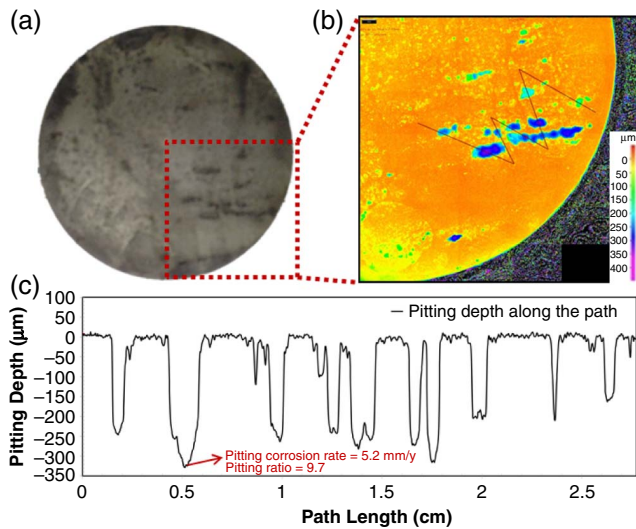


**FIGURE 10.** Pitting depth distribution of the sample from the loop test with 50 wt% MEG at the bottom solution. (a) Sample morphology after the removal of corrosion film; (b) pitting depth distribution measured by profilometer; and (c) pitting depth along the path shown in (b).

liquid fluid at the bottom of line is expected in the upstream. The subsea temperature could also vary in different seasons. So, in this work, the effect of higher MEG content on TLC was also investigated at two subcooling conditions. Table 3 shows the test matrix detailing the experimental conditions of 21 d flow loop corrosion tests with the presence of 70 wt% and 90 wt% MEG.

The results of the average TLC rates, total condensation rate, and MEG content of condensing liquid are given in Figures 11 and 12. The error bars represent the maximum and minimum values of the measured corrosion/condensation rate from replicates. It can be seen that the TLC rates under both high

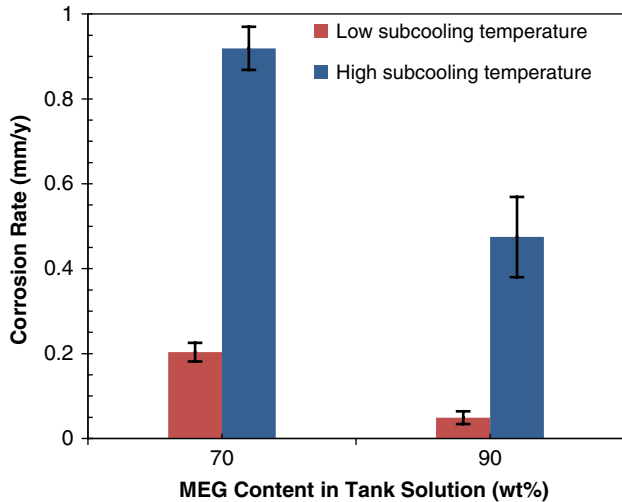
and low subcooling conditions decreased significantly when the MEG content at bottom was increased to 90 wt%. This significant decrease of corrosion rate at 90 wt% MEG can be explained by the strong decrease of the condensation rate and the sharp increase of MEG content at the top of the line, as shown in Figure 12. For the effect of subcooling temperature, higher TLC rates were observed at higher subcooling temperature from both 70 wt% and 90 wt% bottoms MEG content, which can be attributed to the changes of condensation rate and top MEG content.

Inspection of the 90 wt% MEG TLC test samples after the removal of the corrosion products showed uniform corrosion morphology, as shown in Figure 13. In contrast, signs of localized corrosion were observed on the surface of samples taken from the tests with 70 wt% MEG, especially for the samples at high subcooling condition. Figure 14 shows the localized corrosion morphology of the 70 wt% MEG TLC test samples which was analyzed with a 3D profilometer. It is interesting to find that the maximum pitting corrosion rate was greater at the low subcooling temperature than the high subcooling temperature, resulting in an even higher pitting ratio at low subcooling condition. In addition, the characteristics of

**TABLE 3**

Matrix of the 21 d Flow Loop TLC Tests with the Presence of 70 wt% and 90 wt% MEG at Bottom

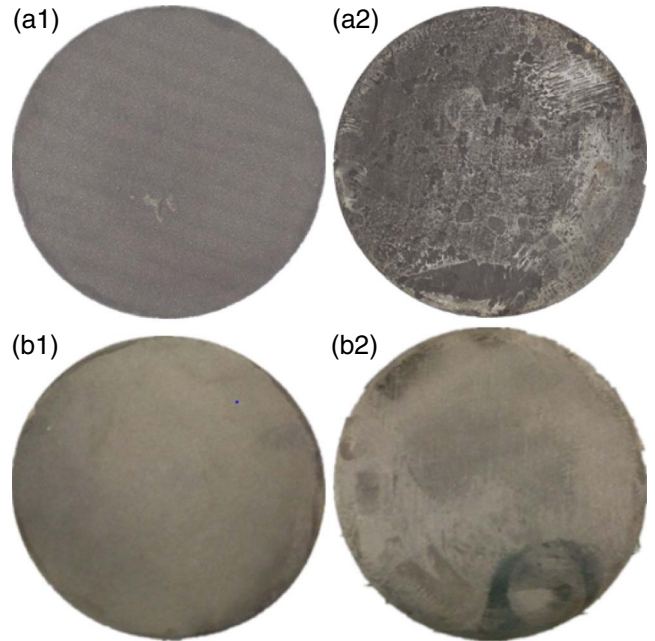
| MEG Content in Tank Solution                              | 70 wt% |      | 90 wt% |      |
|---|--------|------|--------|------|
| Total pressure, $P_{\text{total}}$ (bar)                  | 3      |      |        |      |
| CO <sub>2</sub> partial pressure, $P_{\text{CO}_2}$ (bar) | 2.93   |      | 2.96   |      |
| Gas velocity, $v_{\text{gas}}$ (m/s)                      | 3      |      |        |      |
| Gas temperature, $T_{\text{gas}}$ (°C)                    | 42     |      |        |      |
| Pipe temperature, $T_{\text{pipe}}$ (°C)                  | 40     | 34   | 40     | 34   |
| Subcooling temperature (°C)                               | Low    | High | Low    | High |



**FIGURE 11.** TLC rates at different subcooling temperatures in the presence of 70 wt% and 90 wt% MEG at bottom.

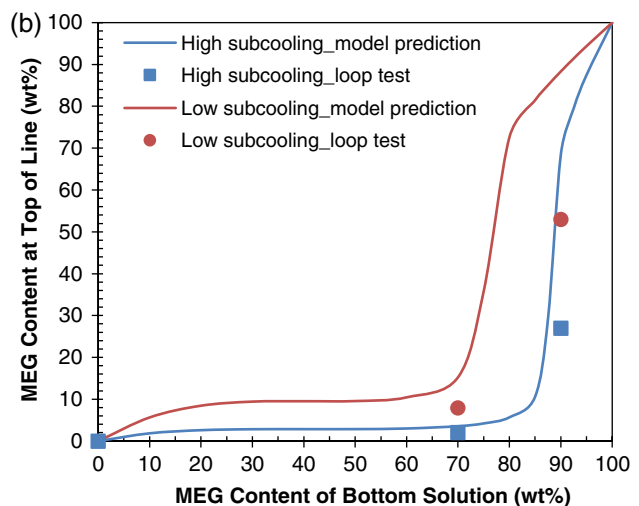
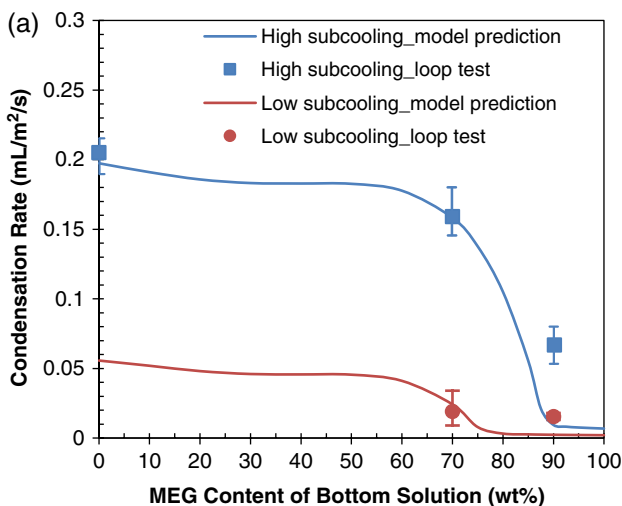
the pits seemed to transform to mesa corrosion morphology at high subcooling temperature, as observed in Figure 14(b).

Figure 15 shows the SEM images of the sample surface and a cross-section view of the corrosion product layer formed on the samples from tests with 70 wt% MEG. For low subcooling condition, the corrosion product layer appeared dense but some gaps could still be observed between adjacent crystalline grains, as shown in Figure 15(a). The SEM cross section (Figure 15[b]) shows clear areas of bare steel within the pit as a sign of high penetration rates. For high subcooling condition, in general the crystalline grains were relatively loosely stacked compared to low subcooling condition and some breakdowns of the layer could be observed in Figure 15(c). Underneath this breakdown area, obvious gaps were found between the corrosion product layer and the bare steel, as



**FIGURE 13.** Pictures of samples after removal of corrosion products. (a) 70 wt% MEG at bottom; (b) 90 wt% at bottom; (1) low subcooling temperature; (2) high subcooling temperature.

observed in the cross-sectional view (Figure 15[d]). Clearly, the layer was not protective in these areas and corrosion easily occurred underneath, which led to wide and flat pits or even mesa corrosion as observed from the profilometer analysis (Figure 14[b]). The EDS analysis shown in Figure 16 suggested the corrosion product layer consists of  $\text{FeCO}_3$  crystals. In addition, some incomplete patterns (indicated by the distribution of the different size of crystals) can be found from the high-resolution SEM images in Figures 15 and 17, which might be caused by the difference of water



**FIGURE 12.** Water and MEG co-condensation results at different MEG content and subcooling temperatures ( $T_{\text{gas}} = 42^\circ\text{C}$ ,  $T_{\text{pipe}} = 34^\circ\text{C}$  for high subcooling,  $T_{\text{pipe}} = 40^\circ\text{C}$  for low subcooling,  $P_{\text{total}} = 3 \text{ bar}$ ,  $v_{\text{gas}} = 3 \text{ m/s}$ ).

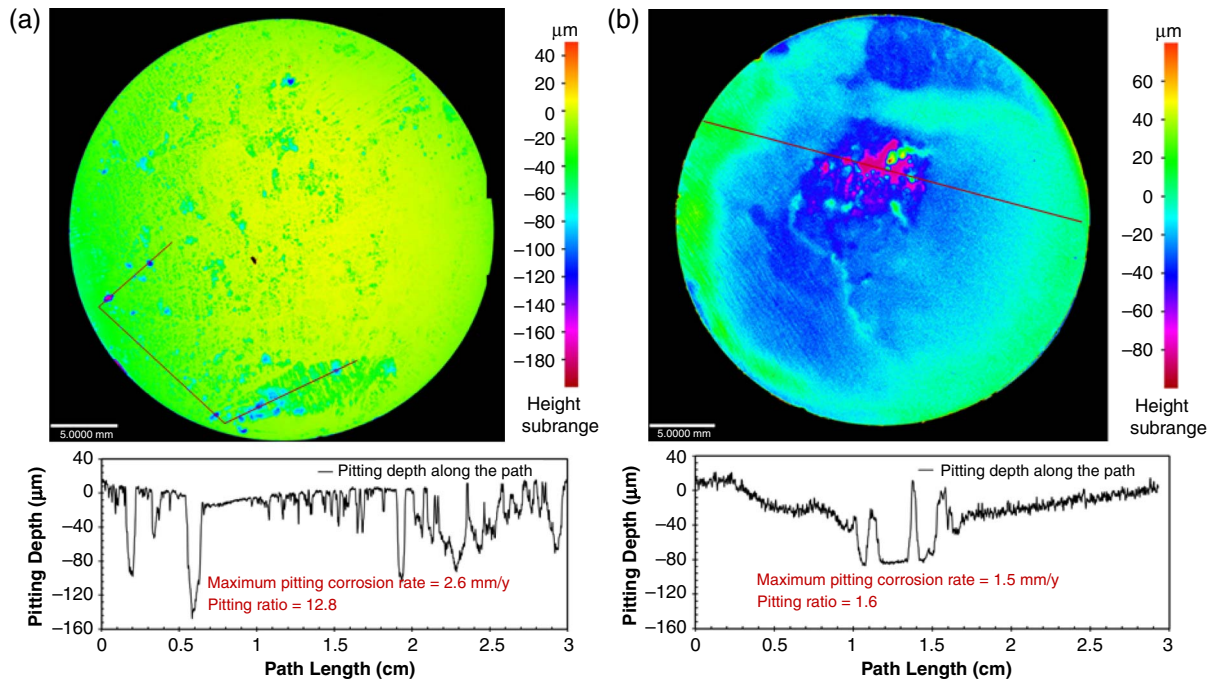


**FIGURE 14.** Pitting depth distribution of samples from the loop corrosion tests with 70 wt% MEG at the bottom: (a) low subcooling temperature; and (b) high subcooling temperature.

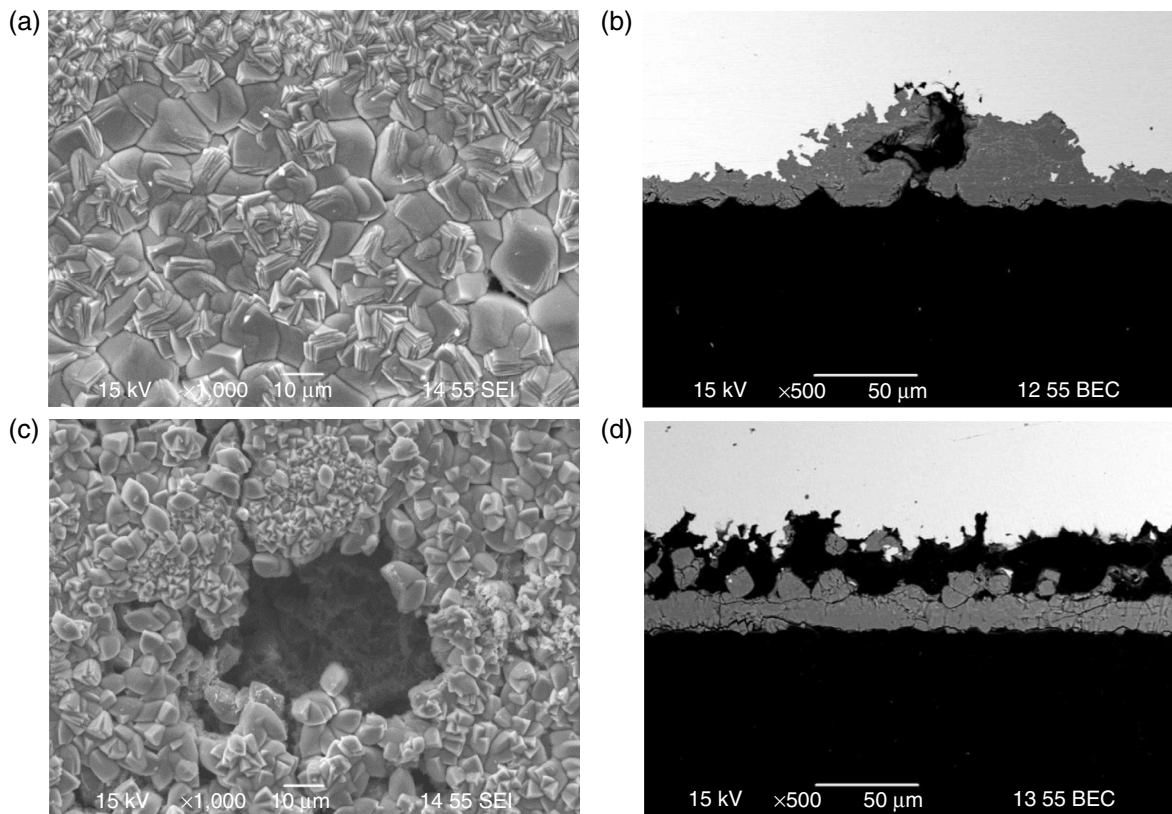


**FIGURE 15.** SEM images of corrosion product layer from loop corrosion test with 70 wt% MEG at bottom: (a) and (b) low subcooling temperature; and (c) and (d) high subcooling temperature.

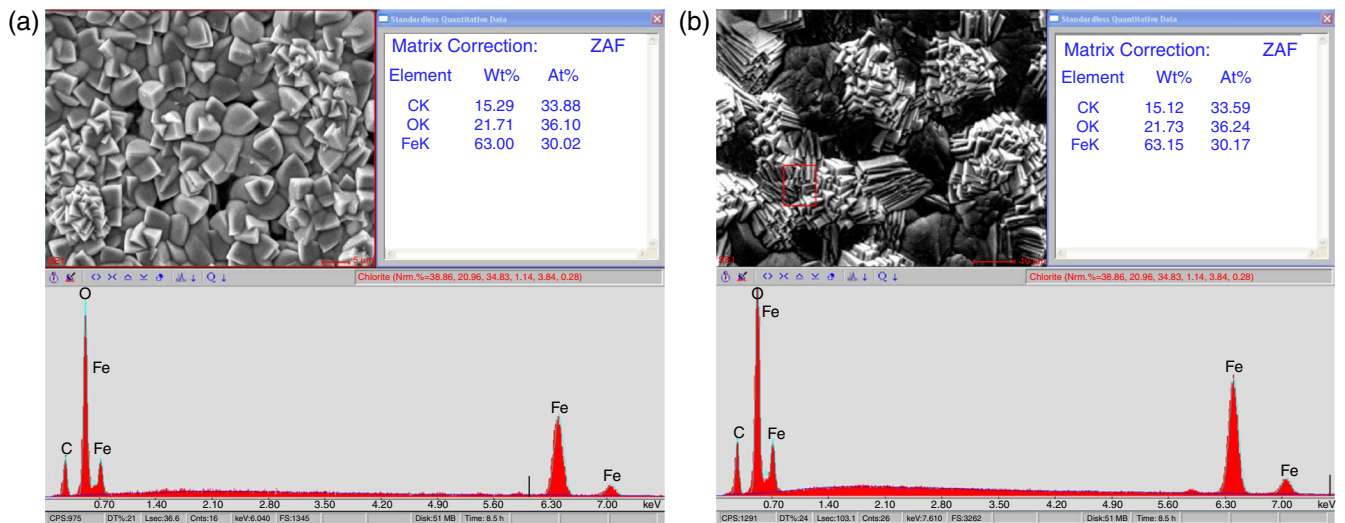


**FIGURE 16.** EDS analysis of corrosion product layer from loop corrosion test with 70 wt% MEG at bottom: (a) low subcooling temperature; and (b) high subcooling temperature.

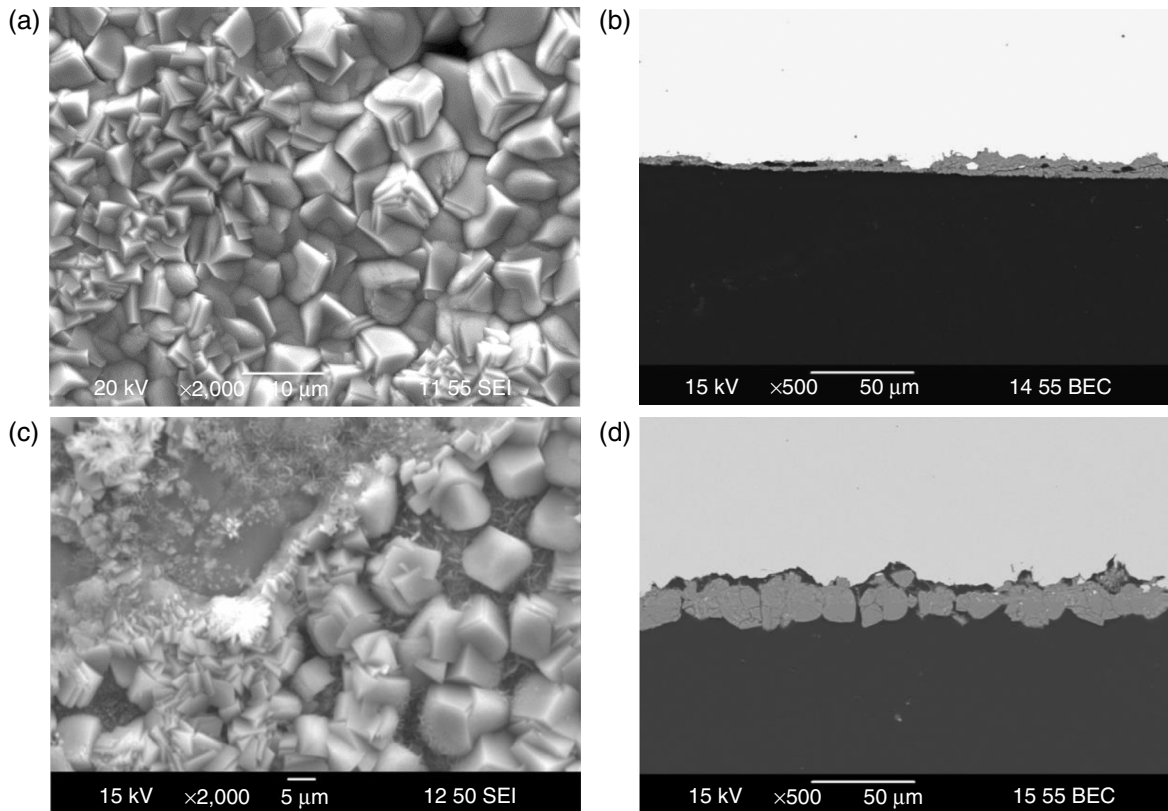


**FIGURE 17.** SEM images of corrosion product layer from loop corrosion test with 90 wt% MEG at bottom: (a) and (b) low subcooling temperature; and (c) and (d) high subcooling temperature.

chemistry inside the droplet and at the interface between adjacent droplets.

The  $\text{FeCO}_3$  corrosion product layer formed on the steel samples from the tests with 90 wt% MEG was also examined by SEM. The SEM images of the surface and cross-sectional views of the formed layer are given

in Figure 17. In general, the corrosion product layer seemed thinner (10 μm to 20 μm) but adherent to the steel surface. Although a few gaps within the layer (Figure 17[b]) and between the layer and the steel surface (Figure 17[d]) could be observed, no localized corrosion was identified. At low subcooling

temperature, the measured condensation rate in presence of 90 wt% MEG was only slightly lower than that at 70 wt% MEG, but the TLC rate and the thickness of the formed layer were much smaller which could be attributed to the inhibition effect of MEG concentration in the condensed liquid. The disappearance of the pitting corrosion at low subcooling temperature when MEG concentration increased from 70 wt% to 90 wt% also indicated the inhibition effect of MEG on localized corrosion. The absence of localized corrosion at high subcooling temperature could be mainly due to the significant decrease of condensation rate in the presence of 90 wt% MEG, as the corrosion product layer seemed to be not protective.

## CONCLUSIONS

- ❖ A mechanistic model was developed to predict the co-condensation process of MEG and water in the presence of noncondensable gases. The predicted condensation rate and MEG concentration in the condensing droplets were in good agreement with experimental results performed in flow loop.
- ❖ The increase of the MEG content at the bottom of the line does not only decrease the total condensation rate, but also increases the MEG content of condensing phase at the top of the line. However, this effect is not pronounced until the MEG content in the bottom liquid phase is higher than 70 wt% to 80 wt%.
- ❖ Long-term experimental results found that the addition of 50 wt% and 70 wt% MEG at the bottom of line had little effect on TLC rate and localized corrosion, while the presence of 90 wt% MEG significantly decreased the TLC rate and no localized corrosion was observed. The corrosion results can be closely attributed to the effect of MEG on the condensation rate and MEG concentration in condensing phase.

## ACKNOWLEDGMENTS

The authors would like to thank the following companies for their financial support: Quadrant Energy, BHP Billiton, BP, Chevron, ConocoPhillips, MI-SWACO, PETRONAS, PTTEP, Woodside, and Repsol.

## REFERENCES

1. D. Hinkson, Z. Zhang, M. Singer, S. Nestic, *Corrosion* 66 (2010): p. 045002-1.
2. P.C. Okafor, S. Nestic, *Chem. Eng. Commun.* 194 (2007): p. 141.
3. M. Singer, A. Camacho, B. Brown, S. Nestic, *Corrosion* 67 (2011): p. 085003-1.
4. M. Singer, J. Al-Khamis, S. Nestic, *Corrosion* 69 (2013): p. 624.
5. Z. Belarbi, F. Farelas, M. Singer, S. Nestic, *Corrosion* 72 (2016): p. 1300.
6. F. Vitse, S. Nestic, Y. Gunalton, D. Larrey de Torreben, P. Duchet-Suchaux, *Corrosion* 59 (2003): p. 1075.
7. M. Singer, D. Hinkson, Z. Zhang, H. Wang, S. Nestic, *Corrosion* 69 (2013): p. 719.
8. M.M. Islam, T. Pojtanabuntoeng, *Corros. Sci.* 111 (2016): p. 139.
9. K.S. Pedersen, M.L. Michelsen, A.O. Fredheim, *Fluid Phase Equilib.* 126 (1996): p. 13.
10. T. Berntsen, M. Seiersten, T. Hemmingsen, *Corrosion* 69 (2013): p. 601.
11. M. Javidi, M. Khodaparast, *J. Mater. Eng. Perform.* 24 (2015): p. 1417.
12. J.-L. Crolet, J.-P. Samaran, "The Use of the Anti-Hydrate Treatment for the Prevention of CO<sub>2</sub> Corrosion in Long Crude Gas Pipelines," CORROSION 1993, paper no. 102 (Houston, TX: NACE International, 1993).
13. C. de Waard, U. Lotz, D.E. Williams, *Corrosion* 48 (1993): p. 976.
14. W. Hayduk, V.K. Malik, *J. Chem. Eng. Data* 16 (1971): p. 143.
15. M.H. Oyevaar, R.W.J. Morsslnkhof, K.R. Westerterp, *J. Chem. Eng. Data* 34 (1989): p. 77.
16. H. Hu, A.T. Kan, M.B. Tomson, *SPE J.* 15 (2010): p. 714.
17. J.N.J.J. Lammers, *Oil Gas J.* 89 (1991): p. 15.
18. B.F.M. Pots, E.L.J.A. Hendriksen, "CO<sub>2</sub> Corrosion Under Scaling Conditions—The Special Case of Top-of-Line Corrosion in Wet Gas Pipelines," CORROSION 2000, paper no. 31 (Houston, TX: NACE, 2000).
19. Z. Zhang, D. Hinkson, M. Singer, H. Wang, S. Nestic, *Corrosion* 63 (2007): p. 1051.
20. J.T. Schrodt, *Ind. Eng. Chem. Process Des. Dev.* 11 (1972): p. 20.
21. J.T. Schrodt, *AIChE J.* 19 (1973): p. 753.
22. Y. Utaka, A. Saito, *Int. J. Heat Mass Transfer* 31 (1988): p. 1113.
23. Z. Zhang, "A Study of Top of the Line Corrosion Under Dropwise Condensation" (Ph.D. diss., Ohio University, 2008), p. 26.
24. J.W. Rose, L.R. Glicksman, *Int. J. Heat Mass Transfer* 16 (1973): p. 411.
25. K. Stephan, *Heat Transfer in Condensation and Boiling* (New York, NY: Springer-Verlag, 1992), p. 84.
26. D.-Y. Peng, B. Robinson, *Ind. Eng. Chem. Fundam.* 15 (1976): p. 59.
27. E.D. Nikitin, P.A. Pavlov, P.V. Skripov, *J. Chem. Thermodynam.* 25 (1993): p. 869.
28. G. Gao, J.-L. Daridon, H. Saint-Guirons, P. Xans, F. Montel, *Fluid Phase Equilib.* 74 (1992): p. 85.
29. T. Pojtanabuntoeng, "Influence of Water/Hydrocarbons Co-Condensation on Top of the Line Corrosion" (Ph.D. diss., Ohio University, 2012), p. 157.
30. D. Veeranna, A. Husain, *Comput. Chem. Eng.* 11 (1987): p. 489.
31. H.S. Naji, *Emirates J. Eng. Res.* 13 (2008): p. 81.
32. C. Mendez, M. Singer, A. Camacho, S. Hernandez, S. Nestic, "Effect of Acetic Acid, pH and MEG on the CO<sub>2</sub> Top of the Line Corrosion," CORROSION 2005, paper no. 278 (Houston, TX: NACE, 2005).
33. M. Singer, "Study and Modeling of the Localized Nature of Top of the Line Corrosion" (Ph.D. diss., Ohio University, 2013), p. 155.